Influence of Pole Shape in Linear Switch Reluctance Actuator Performance

Espírito Santo, A., Calado, M. R., Cabrita C. M.

Department of Electromechanical Engineering, University of Beira Interior, Covilhã, Portugal
aes@ubi.pt, rc@ubi.pt, cabrita@ubi.pt

1. Introduction

Linear Switched Reluctance Actuators (LSRA) exhibits high force/weight ratio with relatively structural simplicity, turning it suitable for robust precision robotics applications [1]. At low speeds this device allow precise motion and speed control. In the lasts years, some proposes had been made concerning linear actuators based on the reluctance variation effect [2,3]. The linear actuator can be constructed in a longitudinal configuration, more robust, with the flux path parallel to the movement. Alternatively the actuator can be constructed in a transversal configuration, and the flux will be transverse to the motion.

As well known, the LSRA can be considered as having two physical structures, being one of them composed by a set of teeth, without coils, and the other one composed by a yoke, with saliencies, poles, which is the coils support [4]. Either the structures can be the stationary or the moving parts. Motion is obtained when the poles intents to minimize the magnetic circuit reluctance. This task produces a tangential force that aligns the poles with the teeth. Because of the desired low speed operation, eddy currents losses are minimum, so magnetic core circuit do not need to be laminated.

A linear bidirectional motion requires a minimum of three stator yokes, in case of independent phase magnetic circuit or three coils sharing the same yoke. Also, a specific sequential power phase feeding is required.

The aim of this paper is to study the influence of polar shape on actuator performance. First, for each polar shape under study, a Finite Elements Model (FEM) is constructed. Static and dynamics simulations are then performed and obtained results presented. Behind the polar shape, no others changes are introduced in the models. Based on the results, an experimental setup is constructed that allows the verification of the FEM results for the more promising polar shapes. Finally, conclusions are taken based on obtained results analysis.

2. LSRA physical presentation

The here under analysis actuator presents a longitudinal configuration. A magnetic yoke and respective coil constitute each actuator phases, being magnetically independent. This characteristic leads to two major advantages: (1) the flux is completely independent for each phase. This is an important aspect because will allow the simultaneous activation of two or more actuator phases without loss of performance due to saturation; and (2) the increasing in the number of phases is possible, increasing also the motion smoothness. Actuator physical structure is presented in Fig.1 with dimensions listed in Table 1. Each phase coil has 1100 turns with 10 Ω.

Table 1: LSRA physical dimensions [mm]

Yoke pole width (a)	10	Air gap length (f)	0.66
Coil length (b)	50	Stator pole width (g)	10
Space between phases (c)	10	Stator slot width (h)	20
Yoke Thickness (d)	10	LSRA length (i)	2000
Yoke pole depth (e)	30	LSRA stack width	35

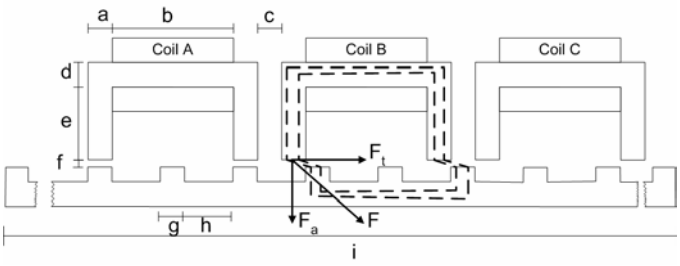

Figure1: LSRA physical structure

3. LSRA Theoretical Working Principle

An electromagnetic device can convert electrical energy into mechanical energy, or vice-versa. This process is made through the device magnetic field.

The design of electromechanical devices requires the prediction of developed force, often derived from field solutions obtained through numerical analysis, based on different approaches [5,6,7], such as (1) classical virtual work; (2) Maxwell stress tensor; (3) Coulomb's virtual work.

Energy is a state function for a conservative system. If losses are ignored, balance energy can be written as in (1), where W_e is the system input energy, W_{fe} the field storage, and f_{em} the mechanical force that produces the mechanical work dW_{em}, when differential displacement dx occurs. Expression (1) also shows that system energy, in a lossless device, depends on flux linkage λ and position x.

$$dW_e = dW_{fe} + f_{em}dx \Leftrightarrow dW_{fe}(\lambda, x) = id\lambda - f_{em}dx \quad (1)$$

A different energy entity, defined as co-energy W_{fe}', without a real physical meaning, can be expressed by (2).

$$W_{fe}'(i, x) = i\lambda - W_{fe} \quad (2)$$

Thus, as can be seen, if a change at linkage flux occurs, the system energy will also change. This variation can be promoted by a means variation in excitation, a mechanical displacement, or both. The coupling field can be

understood as a reservoir of energy stored, that receives it from the entrance system, in this case the electrical system, and delivery it to the exit system, in this case the mechanical system.

After mathematical manipulation of (2), considering (1), (3) is obtained. This expression shows that co-energy W_{fe}' depends on current i and position x:

$$dW_{fe}'(i,x) = \frac{\partial W_{fe}'(i,x)}{\partial i} di + \frac{\partial W_{fe}'(i,x)}{\partial x} dx \quad (3)$$

Because i and x are independent variables, the coefficients in equation (3) are given by (4).

$$\begin{cases} \lambda = \dfrac{\partial W_{fe}'(i,x)}{\partial i} \Rightarrow L = \dfrac{\lambda}{i} \\ f = \dfrac{\partial W_{fe}'(i,x)}{\partial x} \end{cases} \quad (4)$$

4. Finite Elements Static Simulations and Results

Traditional LSRA solutions use a primary and a secondary with rectangular pole shapes, but other polar shapes can be used either in primary or secondary, as for example round or wedge shapes. This work analyses actuator behaviour considering different pole shapes. Figure 2 shows the considered polar configurations.

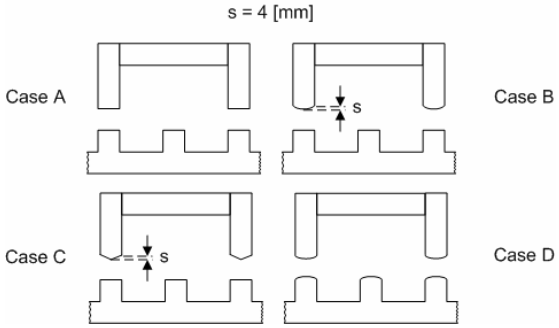

Figure 2: Analysed actuator polar shapes.

For each considered polar shape, a numerical analysis based on FEM was performed [8] (FLUX2D). As an example, the FEM model for Case A is shown at Fig 3. This task allows gathering data, like, beyond others, the magnetic energy, magnetic co-energy, traction force, and inductance.

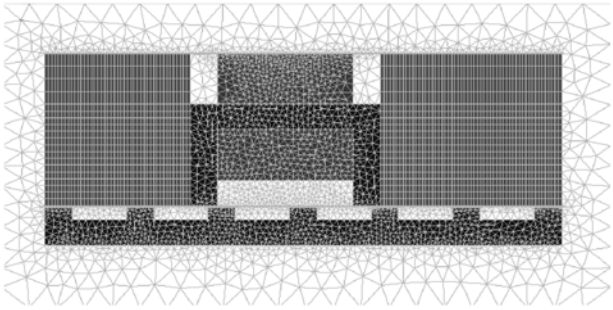

Figure 3: FEM model for Case A.

The here considered stator teeth were always rectangular, with the exception of Case D, for which the shape was round. For a set of primary actuator positions (from x=-15[mm] to x=15[mm] with a 0.25[mm] increment), a set of simulations was performed, with different coil currents (from i=0.25[A] to i=4[A] with an increment of 0.5[A]). Position x=0[mm] corresponds to the alignment between the actuator primary pole and secondary tooth, while positions x=15[mm] and x=–15[mm] correspond to unaligned positions.

The obtained numerical values for the produced actuator traction force (F_t) are shown in Fig. 4, while Fig. 5 shows the obtained numerical values for the produced actuator attraction force (F_a). These figures were obtained with a coil excitation current of 2[A].

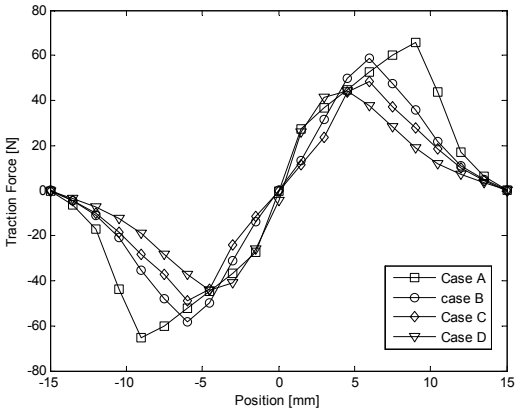

Figure 4: Traction force F_t (i=2[A] /1100 turns).

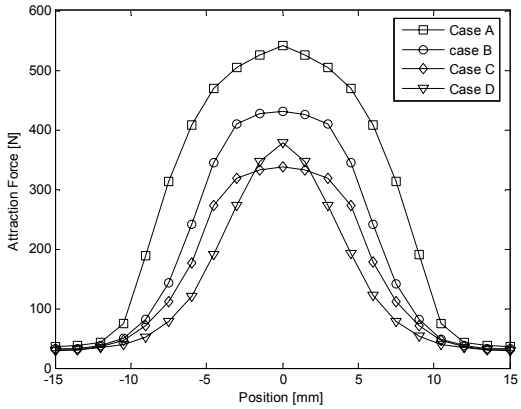

Figure 5: Attraction force F_a (i=2 [A] /1100 turns).

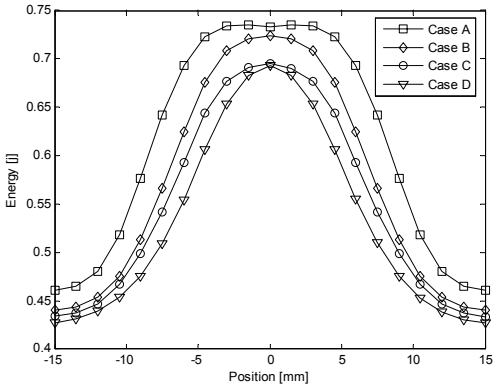

Figure 6: System energy (i=2 [A] /1100 turns).

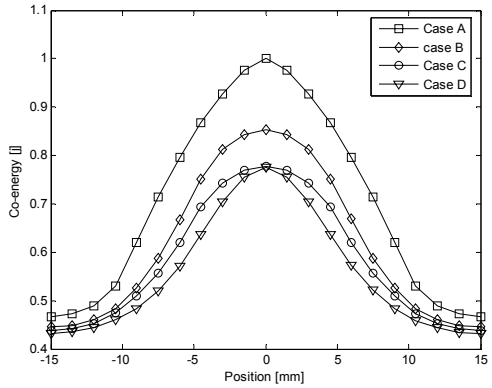

Figure 7: System co-energy (*i*=2 [A] /1100 turns).

Maximum traction force for each considered case is obtained at different positions. For Case A the maximum value was reached at 10 [mm] from the aligned position. In contrast, for Case D the maximum traction force was reached at 5 [mm] from the aligned position.

As we can observe, for each polar shape configuration a different value of attraction force is developed. Case A is the one that exhibits a higher attraction force in a larger band. Case D develops the lower attraction force in a narrow band.

FEM simulations also allowed to observe which way the shape influences the device. A detail of flux density distribution in the polar region for Case C can be observed in Fig 8.

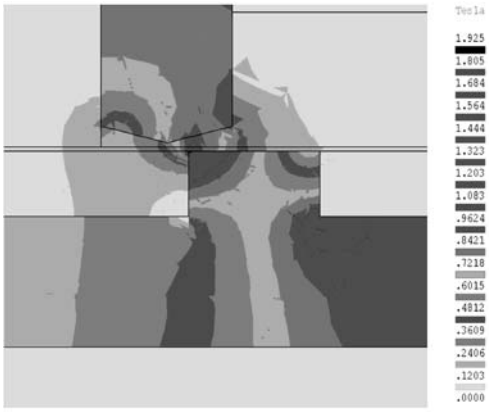

Figure 8: Flux density distribution detail for Case C.

Using the simulation method developed by the authors in [4], where differential equations (5) and (6) represent system dynamics is possible to evaluate polar shape influence in dynamic performance.

Parameters L(i,x) and F_t(i,x) will change not only with position, but also with current. For phase n = {1,2,3}, expression (5) describes electromagnetic behaviour, where R_n is coil's resistance and v_n the supplied voltage.

Mathematical expression (6) describes actuator mechanical behaviour where *a* is the device acceleration, M the actuator mass and F_t the traction force.

$$\begin{cases} v_n = R_n i_n(t) + \dfrac{dL(i_n,x) i_n(t)}{dt} \\ \quad = \dfrac{di_n}{dt}\left[L(i_n,x) + i_n(t)\dfrac{\delta L(i_n,x)}{\delta i}\right] + \dfrac{dx}{dt}\left[\dfrac{\delta L(i_n,x)}{\delta x}\right] + R i_n(t) \end{cases} \quad (5)$$

$$a = \frac{1}{M} F_t \quad (6)$$

A simulation for the excitation of a single-phase is performed with actuator at is initial position (10 [mm] from aligned position), and with a pulse voltage of 30 [V] with a duration of 0.02 [seg].

Fig. 7 shows the response to the pulse voltage. As expected, each polar shape configuration develops a different traction force.

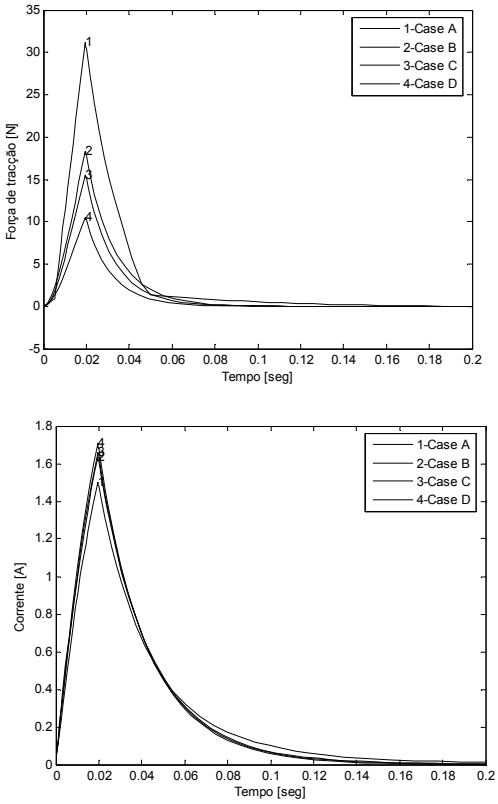

Figure 7: Actuator single-phase excitation current and force (R_n = 10 Ω, v_n=30 V, δt = 0.02 sec, M = 10 kg)

5. Practical Experimental Results

Based on the theoretical obtained results, an experimental setup was built. Caused to the similarity in the obtained results for both Cases B and C, and also because Case D seems to be a relatively technical uninteresting case, the setup experiment was constructed to test only configurations A and B. This setup possesses a mobile platform that supports the actuator primary. Static traction force test is performed leaning the primary platform to a second one, which can be blocked and is equipped with a load cell. Data collected with this experimental setup allowed to verify FEM analysis results.

Fig 9 shows experimental setup with rectangular poles assembled, and Fig. 10 shows a set of round poles that can be assembled in the yoke. Prototype actuator construction

allows to change the primary polar shapes, while all others device physical dimensions are maintained constant, for comparison purposes.

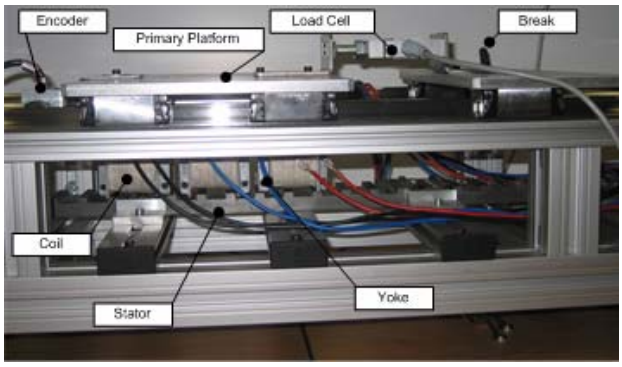

Figure 9: Experimental setup.


Figure 10: Round shape poles.

The experimental setup was used to validate the results obtained with the FEM analysis. The load cell is used to measure the traction force produced by the actuator at fixed positions. Fig. 11 shows the experimental data obtained for the Case A and Case B configurations. Data near the aligned and unaligned position was not obtained because the traction force produced at these positions is very small.

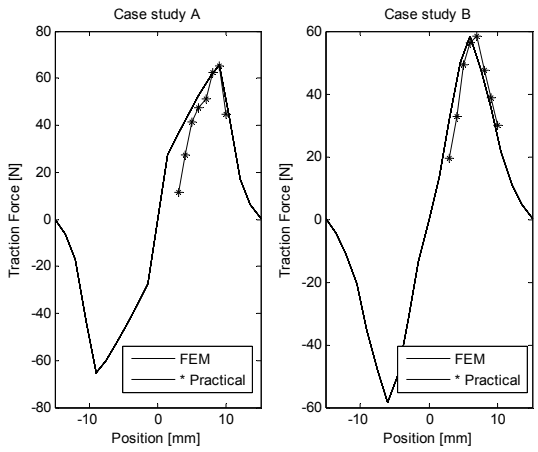

Figure 11: Experimental Traction force F_t (i=2[A] /1100 turns).

6. Results Analysis and Conclusions

The obtained results allowed to conclude that Case B and Case C exhibit a similar behaviour, being the attractive force lower for the second considered case. Also, the developed force F_a in Cases B and C experiment was considerable lower than the produced in Case A. This result is advantageous because one of the actuator design concerns is the maximization of F_t and the minimization of F_a. Traction force F_t development possibility near the aligned position decreases more quickly in Cases B and C, in comparison with Case A. Thus, the influence of current turning off at aligned position is minimized being, in accordance, minimized the actuator's movement ripple and vibration. Case D allows the development of maximum force F_t at positions near the alignment. Thus, the applicability of such a case seems to be uninteresting. For different actuator pole shape configurations, the maximum produced traction force F_t is obtained at different spots. Therefore, the pole shape configuration to be adopted can be choose according to the actuator application and desired performance. The obtained results allow to conclude that the adoption of non-traditionally used pole shapes, round or wedge, leads to a small penalty in traction force and a considerable attraction force minimization. The benefit in actuator effects concerning mechanical structure and performance is evident.

This work is part of a complete drive development for precision position appliance, and these results were considered in the control of the actuator, based in a sliding mode strategy.

References

[1] Chuen Gan, Norbert C. Cheung, Li Qiu. "*Position Control of Linear Switched Reluctance*", IEEE Transactions on Industry Applications, vol. 39, no. 5, september/october 2003.

[2] J. Corda E. Skopljak. "Linear switched reluctance actuator". Sixth International Conference on Electrical Machines and Drives, September 1993.

[3] Han-Kyung Bae, Byeong-Seok Lee, Praveen Vijayraghavan, R. Krishnan,"A Linear Switched Reluctance Motor: Converter and Control", IEEE Transactions on Industry Applications, vol. 36, no. 5, September/October 2000.

[4] A. Espírito Santo, M. R. A. Calado, C. M. P. Cabrita**,** **"**Variable Reluctance Linear Actuator Dynamics Analysis Based on Co-energy Maps for Control Optimization", *Linear Drives for Industry Application*, Kobe-Awaji, 2005.

[5] Mcfee S. and Lowther D.A. (1987): Towards accurate and consistent force calculation in finite element based computational magnetostatics, IEEE Transactions on Magnetics, vol. 23, issue 5, pp. 3771-3773.

[6] Muller W. (1990): Comparison of different methods of force calculation, IEEE Transactions on Magnetics, vol. 26, issue 2, pp. 1058-1061.

[7] Coulomb J. L. (1983): A methodology for the determination of global electromechanical quantities for a finite element analysis and its application to the evaluation of magnetic forces, torques and stiffness, IEEE Transactions on Magnetics, vol.19, issue 6, pp. 2514-2519.

[8] Flux2D Tutorial (Version 7.40), Cedrat, August, 1999.